ACS APPLIED MATERIALS & INTERFACES

Research Article

www.acsami.org

Benzo[1,2-*b*:4,5-*b*′]dithiophene-Based Cruciforms: Syntheses, Crystal Structures, and Charge Transport Properties

Shitao Wang,[†,§] Shendong Ren,[†,§] Yu Xiong,[†] Mao Wang,[†,‡] Xike Gao,[†] and Hongxiang Li*[,†]

[†]Laboratory of Organic Functional Materials & Chemistry, Shanghai Institute of Organic Chemistry, CAS, Shanghai, 200032, China

[‡]School of Materials Science and Engineering, East China University of Science and Technology, Shanghai, 200237, China

Supporting Information

ABSTRACT: Cruciform compound, 2,6-bis(phenylethynyl)-4,8-bis-(phenylethynyl)benzo[1,2-*b*:4,5-*b*′]dithiophene and its alkyl substituted derivatives, **1a−d**, were designed and synthesized. Their physicochemical properties were studied by thermogravimetric analysis, absorption spectra, and cyclic voltammetry. Single crystal diffraction results revealed that **1a−d** adopted different molecular packing in the solid state, which was caused by the introduction and the different orientations of alkyl chains. The single micrometer ribbon transistors of **1a** displayed high mobility up to 0.81 cm^2 V^{-1} s^{-1}. And the as-spun thin film transistors of **1c** exhibited mobility as high as 0.106 cm^2 V^{-1} s^{-1}, 2 orders of magnitude higher than those of **1b** (0.006 cm^2 V^{-1} s^{-1}) and **1d** (0.002 cm^2 V^{-1} s^{-1}).

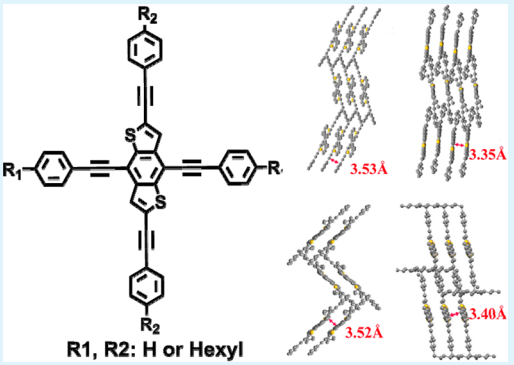

KEYWORDS: *cruciform, transistors, molecular packing, mobility*

INTRODUCTION

Organic field-effects transistors (OFETs) are the basic elements of organic electronics and have found wide applications in radio frequency identification tags (RFID),[1] flexible displays,[2] electronic papers,[3] sensors,[4] and so forth. OFETs consist of an organic semiconductor (OSC) layer, dielectric layer, and electrodes. Among them, OSCs are the key component to determine the performance of OFETs. Though great progress has been made in OSCs recently and OSCs with mobility higher than amorphous silicon have been reported,[5] there is still a great need to design and synthesize a new type of high performance OSCs to ensure the practical applications of OFETs. Moreover, the fundamental knowledge regarding the relationship between organic semiconductor's structure and device performance is still immature. So it is crucially significant to develop new types of high-performance OSCs and systematically investigate their structure−property relationships.

The charge transport property of OSCs is strongly affected by their molecular packing in the solid state. Theoretical and experimental results showed lamellar $\pi-\pi$ stacking structures facilitated charge transport.[6,7] However, most of the OSCs adopted herringbone structure in the solid state,[8] and until now it is still a great challenge to tune the molecular packing of OSCs.[9] In this manuscript, by introducing alkyl chains and changing the orientation of alkyl chains, the tune of molecular packing of OSCs from herringbone structure with large herringbone angle to herringbone structure with small herringbone angle and finally lamellar packing mode was achieved.

Cruciform compounds have received significant attention because of their unique shapes and properties and have been used in sensors, nonlinear optical materials, and OFETs.[10] Neher et al. prepared series of oligothiophene type cruciforms (for the chemical structure, see Scheme 1), a mobility up to 0.012 $cm^2/(V\ s)$ was observed based on solution processed thin film transistors.[11] We synthesized anthracene-containing cruciform **BPEA** (for the chemical structure, see Scheme 1), and the single crystal transistor of **BPEA** displayed mobility as high as 0.73 $cm^2/(V\ s)$.[12] Recently, Choi et al. reported the spin-coated thin films of 2,6,9,10-tetrakis(phenylethynyl)anthracene (**TPEA**) (for the chemical structure, see Scheme 1) showed high mobility up to 0.27 cm^2 V^{-1} s^{-1} under ambient conditions.[13] Inspired by these exciting results, herein new type of cruciform OSCs **1a−d** (for the chemical structures, see Scheme 2) were designed and synthesized. Compounds **1a−d** have the following merits: (1) employing triple bonds to afford large conjugation length and good planarity; (2) introducing alkyl chains on the different positions of cruciforms, which can systematically investigate the impact of alkyl chain orientations to molecular packing and the structure−property relationships of cruciform type OSCs. Experimental results showed the introduction and the orientation of alkyl chains strongly affected the molecular packing of **1a−d**. Transistor characteristics were exhibited by the single micrometer ribbon transistors of **1a** which displayed high mobility up to 0.81 cm^2 V^{-1} s^{-1}.

Received: September 26, 2012
Accepted: December 30, 2012
Published: December 30, 2012

Scheme 1. Chemical Structures of Some Reported Cruciform OSCs

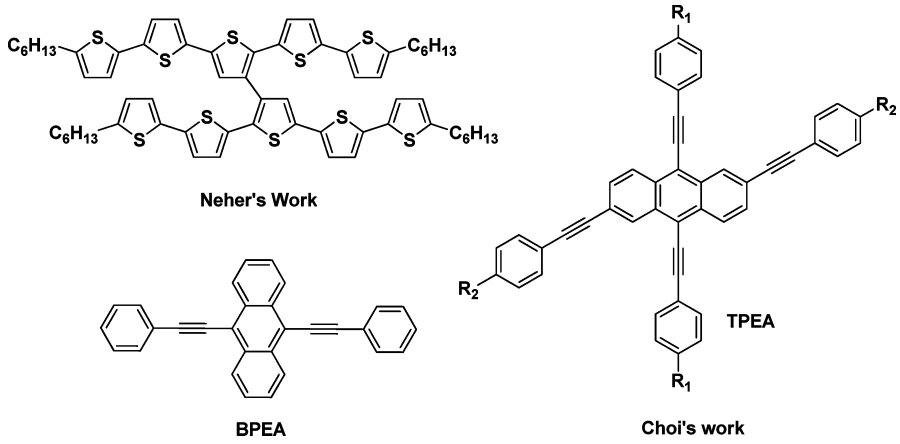

Scheme 2. Synthetic Route and Chemical Structures of 1a−d

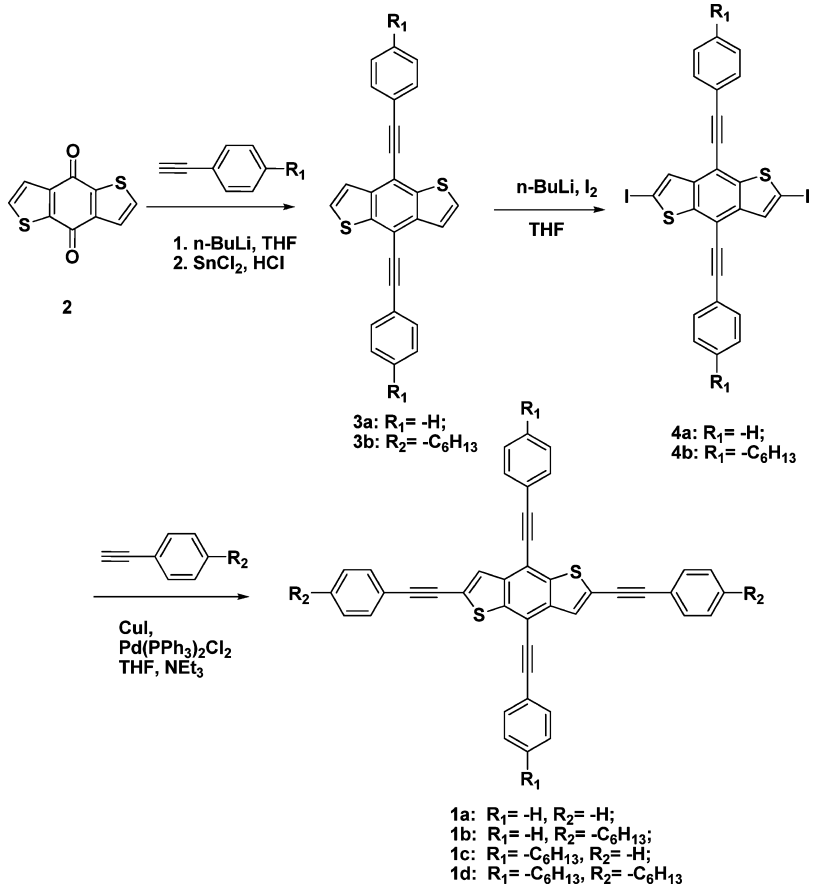

And, the spin-coated thin film transistors of **1c** showed mobility as high as 0.106 $cm^2 V^{-1} s^{-1}$, 2 orders of magnitude higher than those of **1b** and **1d**, demonstrating the strong effect of alkyl chains to OSCs performance.

RESULTS AND DISCUSSION

The synthetic route of compounds **1a−d** was shown in Scheme 2. Commercially available diketone **2** reacted with corresponding phenylacetylene derivatives, followed by aromatization in the presence of tin chloride to afford compound **3**.[14] Compound **4** was prepared by treating **3** with *n*-BuLi and excess iodine. And the final cruciform compounds **1a−d** were synthesized through palladium-catalyzed Sonogashira coupling reactions of **4** with corresponding phenylacetylene derivatives. Compounds **1b−d** displayed moderate solubility in organic solvents such as $CHCl_3$, THF, and chlorobenzene. All the target compounds were purified twice by recrystallization (for **1a−c**) and flash chromatography (for **1d**) prior to further characterization.

The thermal properties of compounds **1a−d** were characterized by thermogravimetric analysis (TGA) as shown in Figure 1. TGA results revealed that all compounds had good thermal stabilities with insignificant weight loss up to 400 °C. The onset decomposition temperatures were 500, 425, 425, and 423 °C for **1a−d**, respectively, decreasing with the introduction

dx.doi.org/10.1021/am302117k | ACS Appl. Mater. Interfaces 2013, 5, 663−671

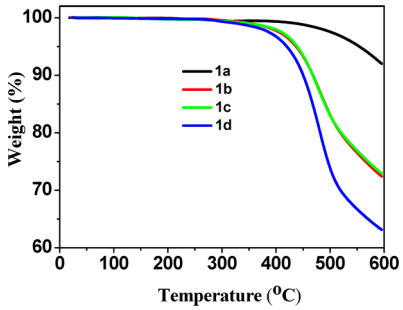

Figure 1. TGA plots of **1a**–**d** with a heating rate of 10 °C min^{-1} under N_2.

of alkyl chains. Compound **1b** and **1c** exhibited identical thermal decomposition curves, indicating the orientation of alkyl chains had little effect on the thermal property of materials.

Figure 2 illustrated the normalized UV–vis absorption spectra of **1a**–**d** in dilute chloroform solution and in solid

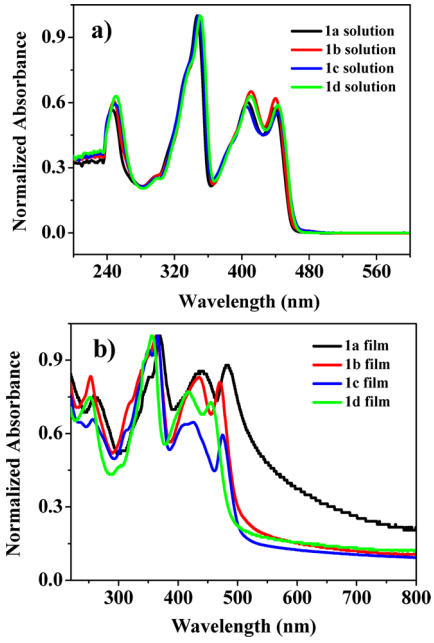

Figure 2. Normalized UV–vis absorption spectra of **1a**–**d** in dilute chloroform solution (1×10^{-4} mol/L) (a) and thin film (b) on quartz substrates. All absorption spectra were measured at room temperature.

thin films. All compounds had the approximately identical UV–vis absorption spectra in solution with four main absorption peaks at around 250, 350, 410, and 440 nm. The optical band gaps of **1a**–**d** estimated from the initial absorptions of the solution spectra were 2.69, 2.68, 2.66, and 2.67 eV, respectively. The absorption spectra indicated that the alkyl chains and their orientations did not distinctly affect the HOMO–LUMO energy gap of cruciforms. The absorptions of **1a**–**d** in the films were apparently red-shifted compared with those of solutions, suggesting J- aggregations were the dominant packing mode in the solid states.[15] The onset absorptions of **1b**–**d** films showed ~40–50 nm red shift, while that of **1a** was shifted ~100 nm,[16] which indicated the intermolecular interactions of **1a** were stronger than those of **1b**–**d**. The fluorescence emission spectra of **1a** and **1b** in dilute THF solution displayed nearly identical spectra with a maximum emission at 453 nm and a shoulder at 484 nm. The spectra of **1c** and **1d** were similar as those of **1a** and **1b**, but the emission peaks were slightly red-shifted ~5 nm (maximum emission: 458 nm and a shoulder at 489 nm; see the Supporting Information). The emission spectra further confirmed that the alkyl chains and their orientations had little influence on the HOMO–LUMO energy gap of **1a**–**d**.

Cyclic volatmmetry of compounds **1a**–**d** were conducted under N_2 in 0.1 M Bu_4NPF_6/CH_2Cl_2 solution by using ferrocene as the internal standard (Figure 3). **1a**–**d** exhibited a quasi-reversible redox peak. The onset oxidation potentials of **1a**–**d** were 1.27, 1.22, 1.23, and 1.19 eV, respectively. The HOMO energy levels calculated through the equation $E_{HOMO} = -[4.8 - E_{FOC} + E_{ox}^{1/2}]$ eV (The HOMO energy level of ferrocene was −4.80 eV)[17] were −5.66 eV for **1a**, −5.61 eV for **1b**, −5.62 eV for **1c**, and −5.58 eV for **1d**. These values were very close to that of linear compounds 2,6-bis((4-hexylphenyl)-ethynylene)benzo[1,2-*b*:4,5-*b*]dithiophene (−5.63 eV),[18] indicating that the introduction of alkyl substituted aryl-acetylene slightly affected the HOMO energy levels of cruciforms. Combing with absorption spectra, the LUMO energy levels of **1a**–**d** were calculated as −2.97, −2.93, −2.96, and −2.91 eV, respectively.

Single crystal X-ray diffraction analysis was carried out to investigate the intermolecular interactions and arrangement patterns of **1a**–**d** (Figure 4). Orange needle-shaped single crystals of **1a**–**d** were prepared by the solvent vapor diffusion method from THF/methanol, THF/methanol, chloroform/ethanol, chloroform/methanol solutions, respectively. XRD results revealed **1a**–**c** adopted typical herringbone structure with herringbone angles of 37.4, 12.2, and 88.5°. Moreover, strong π–π interactions between neighboring molecules, namely slipped π–π stacking, were observed in **1a**–**c** single crystals. For **1a**, the single crystals belonged to a monoclinic space group $P2_1/n$ with unit-cell parameters of a = 3.926(2) Å, b = 29.897(15) Å, c = 12.602(7) Å, β = 96.092(9)°. The distances of the neighboring face-to-face molecules were around 3.53 Å with large π–π overlap areas. The single crystals of **1b** and **1c** had the same monoclinic space group $P2_1/c$. The single crystals of **1b** had unit-cell parameters of a = 9.453(3) Å, b = 23.472(8) Å, c = 10.814(4) Å, and β = 115.077(6)°. The π–π distance was ~3.35 Å, shorter than that of **1a**. However, the π–π overlap area of **1b** was smaller than that of **1a**. For the single crystals of **1c** which has alkyl chains along the short conjugated axis, the unit cell parameters were a = 19.400(2) Å, b = 5.0590(6) Å, c = 22.602(3) Å, β = 102.273(3)°. The π–π distance between neighboring molecules was about 3.52 Å, nearly the same as **1a**. And the π–π overlap area of **1c** was smaller than that of **1a** and larger than that of **1b**.

By contrast, the single crystal packing model of **1d** was triclinic space group $P\bar{1}$ with unit cell parameters of a = 8.6659(17) Å, b = 13.122(3) Å, c = 13.694(3) Å, α = 112.960(4)°, β = 93.861(4)°, γ = 97.858(4)°. The packing pattern of **1d** was totally different with those of **1a**–**c** (Figure 4). **1d** adopted the lamellar packing motif with an intermolecular distance between neighboring face-to-face molecules around 3.40 Å, and the overlap area was nearly the same as that of **1b** but much lower than those of **1a** and **1c**. In the different packing model, π–π overlap areas as well as π–π distances of **1a**–**d** in single crystals suggested the crucial effect of alkyl chains on molecular packing.

The molecular arrangement of **1a**–**d** in thin films was investigated by X-ray diffraction (XRD). Due to poor solubility, **1a** formed crystalline micrometer sized ribbons instead of

dx.doi.org/10.1021/am302117k | ACS Appl. Mater. Interfaces 2013, 5, 663–671

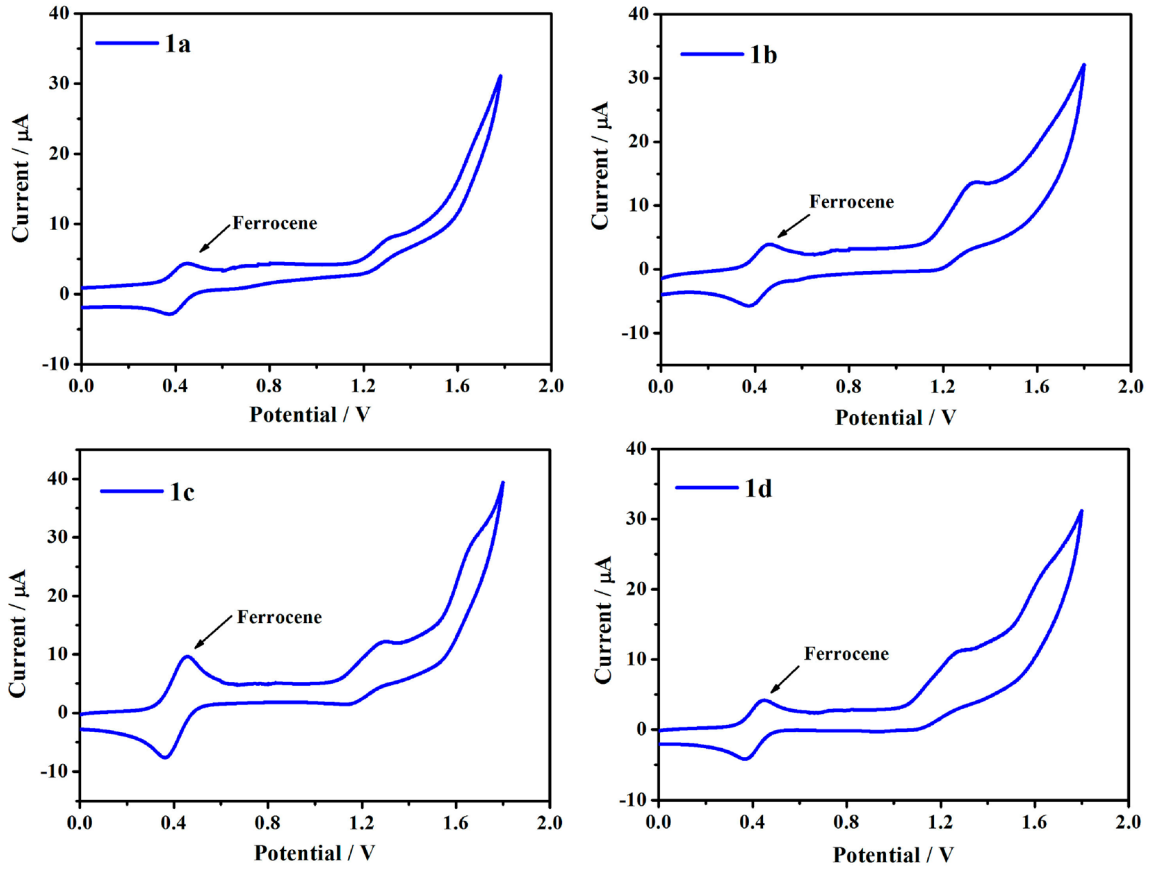

Figure 3. Cyclic voltammograms of **1a**, **1b**, **1c**, and **1d** in CH_2Cl_2 solutions with SCE as the reference electrode, ferrocene as the internal standard, and scan rate of 100 mV/s.

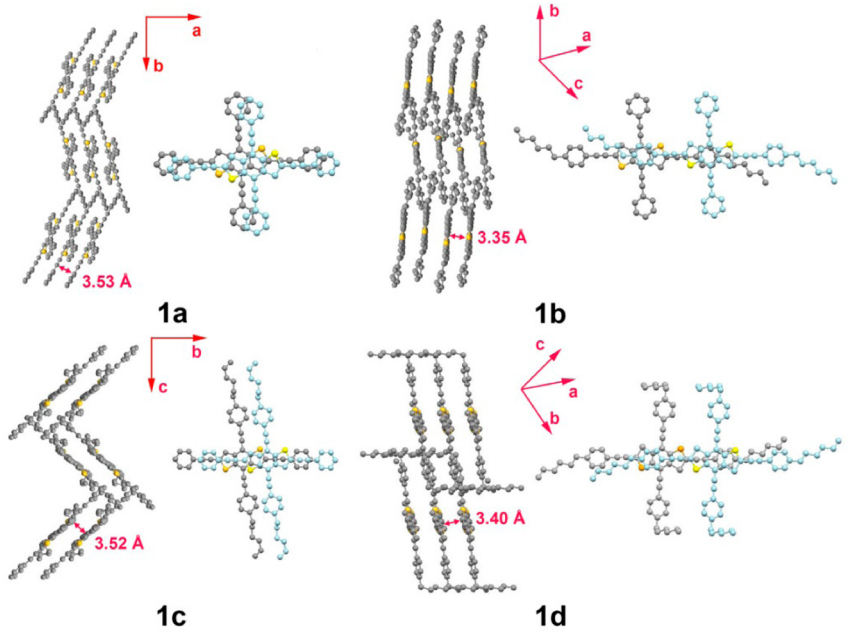

Figure 4. Single-crystal structures and $\pi-\pi$ stackings of **1a**–**d**. Hydrogen atoms were removed for clarification.

successive films. The ribbons have a length from tens to hundreds of micrometers and a width from hundreds of nanometers to several micrometers. Figure 5 illustrated the XRD pattern of **1b**–**d** thin films and **1a** micrometer ribbons. As for **1a**, the molecules adopted same packing in the ribbons as that of single crystals. Additionally, the straight baseline and sharp diffraction peaks suggested the high quality of **1a** ribbons. The *d*-spacing determined from the main reflection peaks (010) was 29.35 Å, which was very close to the cell length of *b* axis (29.897 Å) in the corresponding single crystals, suggesting that

dx.doi.org/10.1021/am302117k | ACS Appl. Mater. Interfaces 2013, 5, 663–671

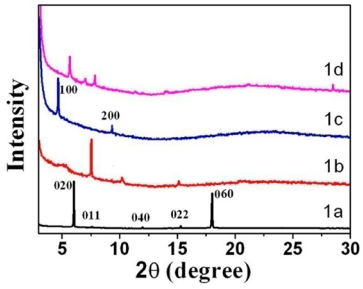

Figure 5. XRD patterns of the **1a** ribbons and **1b–d** thin films.

in the ribbon **1a** had the *b* axis nearly perpendicular to the substrate surface as shown in Figure 6a. With this orientation, the $\pi-\pi$ stacking direction was parallel to the substrate surface according to the single crystal structure. Theoretical calculation based on the Bravais–Friesdel–Donnay–Harker (BFDH) method showed that **1a** strongly tended to form one-dimensional ribbons. In the ribbons, the $\pi-\pi$ stacking was along the ribbon's growth direction, which was the same as we proposed from the XRD result. The diffraction peaks of compound **1c** also corresponded well with the reflections of the single-crystals and the *d*-spacing determined from the reflection peaks were 18.82 Å, close to the cell length of *a* axis (19.40 Å) in the single crystals. Therefore, we inferred that the **1c** crystallites of the films had the *a* axis slightly tilted to the substrate surface (Figure 6b). Both **1b** and **1d** thin films exhibited multiple reflection peaks, suggesting the highly crystalline property of the thin films. However, differently with **1a** and **1c**, the packing of **1b** and **1d** in the thin films were not the same as that of single crystals, indicating new phases were formed in the thin films.

Figure 7 showed the AFM images of **1b–d** thin films and **1a** micrometer ribbons. The surface of the ribbons which were grown from chlorobenzene (50 °C) on SiO_2/Si substrate was very smooth, suggesting the high quality of the ribbons. Compound **1b** formed continuous films and the morphology of the films displayed granular features with certain terrace structures. The morphology of **1c** thin films was apparently different with that of **1b** and exhibited rod-like grains with partial orientations, further proving the effect of alkyl substituents orientation on molecular packing. Ordered ribbon-like features were observed for the thin films of **1d**; however, **1d** reassembled to uncontinuous micronano-sized fibers when **1d** thin films were stored at room temperature for a few hours or heated to ~50 °C, which we believe was due to the low melt point of **1d** (see the Supporting Information).

In order to investigate the charge transport properties of **1a–d**, bottom–gate top-contacted transistors of **1a–d** were fabricated. A heavily n-doped Si wafer was served as the gate electrode. A thermally grown 300 nm SiO_2 layer (the specific capacitance was measured to be 10 nF cm^{-2}) was used as the dielectric layer. All of the devices were fabricated and tested in ambient condition. The mobility of devices was calculated on the saturated region according to the expression $I_{DS} = (W/2L)\mu_+C_i(V_G - V_{Th})^2$, where L and W are the channel length and width, respectively, and C_i is the capacitance. All transistors exhibited p-channel characteristics. Figure 8 showed the typical transfer curves of **1a** and **1c** transistors (The output and transfer curves of **1a–d** transistors were given in the Supporting Information). The performance of the transistors was summarized in Table 1.

The single micrometer ribbon transistors of **1a** displayed high device performance with mobility as high as 0.81 $cm^2\ V^{-1}\ s^{-1}$ and on/off current ratio to $10^5–10^6$, which was due to the

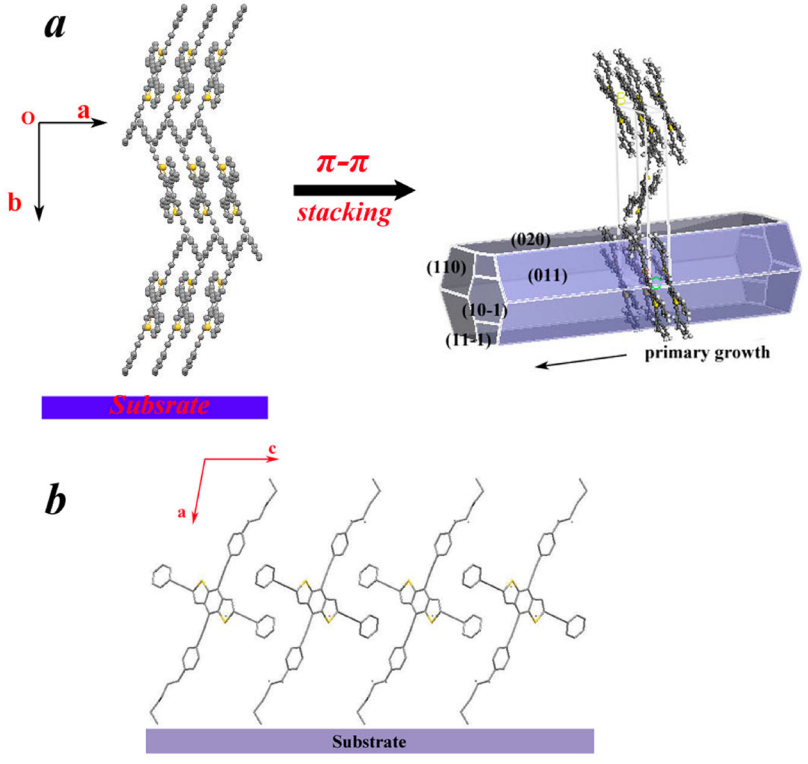

Figure 6. Proposed molecular stacking model of **1a** (a) and **1c** (b) in the thin film.

dx.doi.org/10.1021/am302117k | ACS Appl. Mater. Interfaces 2013, 5, 663–671

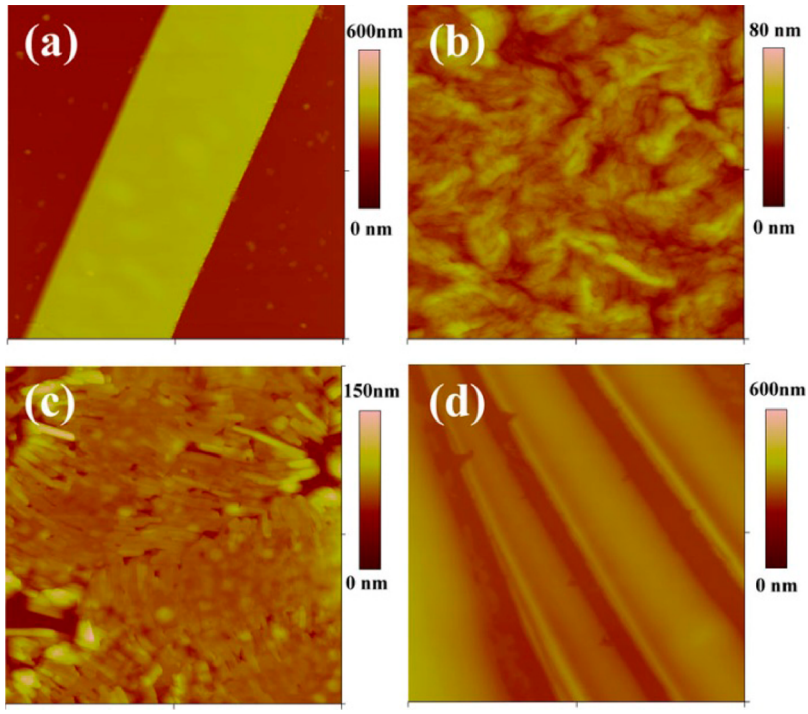

Figure 7. AFM images (5 μm × 5 μm) of ribbons **1a** (a) and thin films **1b** (b), **1c** (c), and **1d** (d).

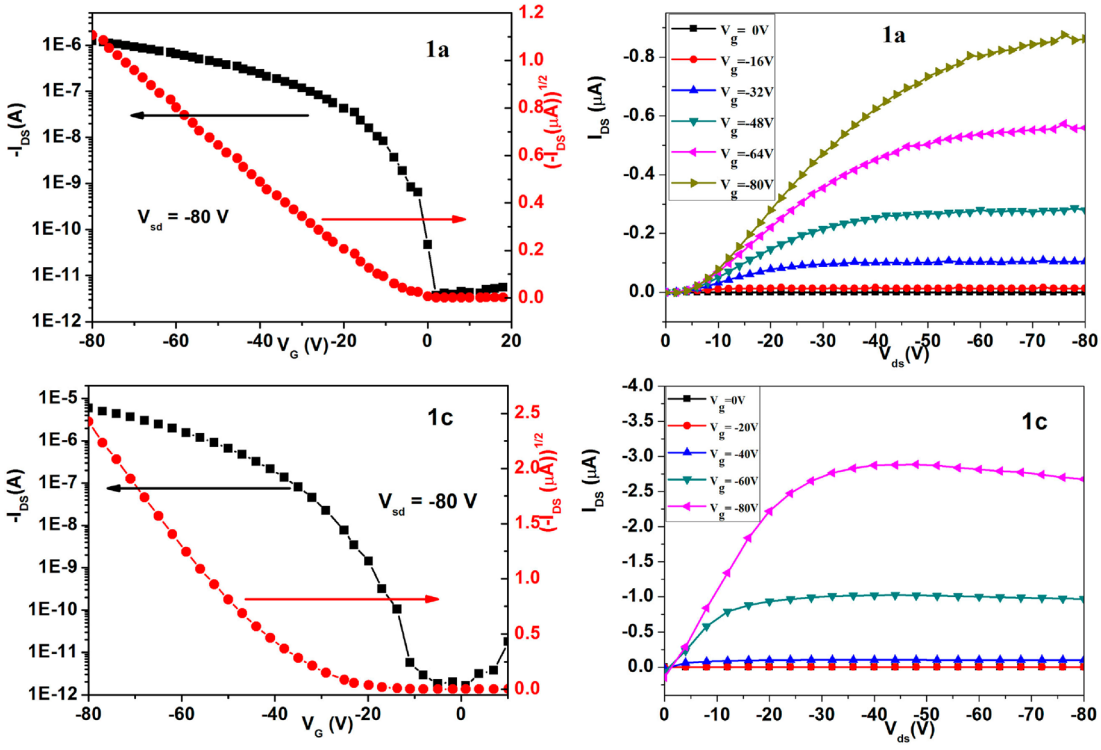

Figure 8. Transfer (left) and output (right) curves of **1a** single ribbon transistor (W/L = 0.2) and **1c** thin film transistor.

high quality of the ribbons. The average mobility of the thin film transistors of **1b** and **1d** was 0.003 and 0.001 $cm^2\ V^{-1}\ s^{-1}$, respectively. Compound **1c** exhibited the highest performance among **1b**–**d** thin film transistors. The average mobility of **1c** was 0.073 $cm^2\ V^{-1}\ s^{-1}$, and the highest mobility was up to 0.106 $cm^2\ V^{-1}\ s^{-1}$, 2 orders of magnitude higher than those of **1b** and **1d**. The excellent mobility of **1c** thin film transistors was ascribed to (1) the large π–π overlap area and the ordered molecular packing of **1c** in thin films which facilitated charge transport; (2) the high quality of the thin films; and (3) the continuous and partial orientated rod-like features in thin films.

CONCLUSION

In conclusion, cruciform compound **1a** and its alkyl substituted derivatives **1b**–**d** were strategically designed and synthesized. The single crystal X-ray diffraction results revealed the

dx.doi.org/10.1021/am302117k | ACS Appl. Mater. Interfaces 2013, 5, 663–671

Table 1. Transistor Performances of Cruciform OSCs 1a−d Measured at Room Temperature in Ambient Conditions

compound	μ (cm^2 V^{-1} s^{-1})[b]	V_{Th} (V)[c]	I_{on}/I_{off}
1a[a]	0.22 (0.81)	−16	10^5−10^6
1b	0.003 (0.006)	−62	10^4−10^5
1c	0.073 (0.106)	−42	10^6−10^7
1d[a]	0.001 (0.002)	−3	10^5−10^6

[a]Source and drain electrodes were prepared using the "gluing Au films" method.[19] [b]The values are average mobility and the maximum mobility (in parentheses). [c]Average threshold voltage for at least 12 devices.

molecular packing and intermolecular interactions of **1a−d** were apparently different, suggesting the strong effect of alkyl chains and their orientations to the intermolecular interactions and the molecular packing. Compounds **1b−d** could form continuous crystalline thin films while **1a** formed micrometer ribbons through solution process technique. The transistors of single micrometer ribbons of **1a** exhibited high device performance with hole mobility up to 0.81 cm^2 V^{-1} s^{-1}. The as-spun thin film transistors of **1c** displayed hole mobilities as high as 0.106 cm^2 V^{-1} s^{-1}, 2 orders of magnitude higher than those of **1b** and **1d**. These results suggested the potential applications of cruciform OSCs in organic electronics and provided very useful information for the investigation of structure−property relationship of cruciform type semiconductors.

EXPERIMENTAL SECTION

General Information. ^1H and ^{13}C NMR spectra were obtained in $CDCl_3$ on varian Mercury (300 or 400 MHz) instrument with TMS as internal reference and peak multiplicity was reported as follows: s, singlet; d, doublet; t, triplet; m, multiplet. Mass spectra (EI-MS) were carried out on a Shimadzu Qp-5050A Spectrometer using an electron impact ionization procedure (70 eV) and MALDI-TOF spectra were carried out on a Voyager-DE STR Mass Spectrometer. Elemental analyses were performed on an Elementar Vario EL III elemental analyzer. Absorption spectra were measured on a U-3900 UV−vis spectrophotometer. Melting points were determined by an X-4 microscopic melting point apparatus. Cyclic voltammetric measurements were carried out in a conventional three-electrode cell using a platinum button working electrode, a platinum wire counter electrode, and a saturated calomel electrode (SCE) reference electrode on a computer-controlled CHI610D instruments. X-ray diffraction (XRD) measurements were carried out in the reflection mode using a 2-kW Rigaku X-ray diffraction system. Atomic force microscopy (AFM) was recorded on a Nanoscope IIIa AFM in tapping mode. TGA was conducted with a PerkinElmer Pyris 1 TGA and were carried out on approximately 6−8 mg film samples heated in flowing nitrogen at a heating rate of 10 °C/min.

Syntheses. 1-Ethynl-4-hexylbenzene was synthesized according to the literature.[18] All other chemicals and solvents were purchased from Aldrich, Alfa Aesar, Puyang Huicheng Chemicals Co. Ltd. and Sinopharm Chemical Reagent Co. Ltd.

Synthesis of Compound 3a. Phenylacetylene (3.000 g, 0.0294 mol) was dissolved in freshly distilled THF (50 mL) at 0 °C. *n*-Butyl lithium (2.4 M) in hexane (12.5 mL, 0.030 mol) was added dropwise, and the solution was stirred at 0 °C for 30 min followed by the addition of 4,8-dihydrobenzo[1,2-*b*:4,5-*b*′]dithiophen-4,8-dione (**2**) (2.951 g, 0.0134 mol) dissolved in THF (50 mL). After addition, the reaction mixture was heated at reflux for 1 h. Then, the mixture was cooled to 0 °C and tin chloride dihydrate ($SnCl_2·2H_2O$) (3.85 g, 0.0171 mol) dissolved in HCl solution (20%, 50 mL) was added. After that, the reaction mixture was heated to reflux for 2 h. After being cooled to room temperature, the mixture was diluted with chloroform and the organic layer was washed with water, dried with magnesium sulfate, filtered, and concentrated to reddish solution (10 mL) which was added to an excess of methanol. Recrystallization from toluene afforded **3a** as yellow solid (3.200 g, 55.8%). ^1H NMR (400 MHz, $CDCl_3$, 25 °C, TMS): δ 7.72 (d, ^3J(H,H) = 5.6 Hz, 2H), 7.69 (m, 4H), 7.59 (d, ^3J(H,H) = 5.6 Hz, 2H), 7.41 ppm (m, 6H). ^{13}C NMR (400 MHz, $CDCl_3$, 25 °C, TMS): δ140.37, 138.24, 131.78, 128.84, 128.49, 128.16, 123.21, 122.85, 112.00, 99.20, 85.65 ppm. MS (EI): 390 [M^+]. HRMS (EI) *m*/*z* calcd for $C_{24}H_{14}S_2^{+1}$: 390.0537. Found: 390.0533. Elemental analysis calcd (%) for $C_{24}H_{14}S_2$: C 79.96, H 3.61. Found: C 79.74; H 3.87.

Synthesis of Compound 3b. Compound **3b** was synthesized in 48.9% yield in a manner similar to that described for **3a**. ^1H NMR (300 MHz, $CDCl_3$, 25 °C, TMS): δ7.71 (d, ^3J(H,H) = 5.7 Hz, 2H), 7.60 (d, ^3J(H,H) = 8.4 Hz, 4H), 7.57 (d, ^3J(H,H) = 5.7 Hz, 2H), 7.23 (d, ^3J(H,H) = 8.4 Hz, 4H), 2.66 (t, ^3J(H,H) = 7.5 Hz, 4H), 1.64 (m, 4H), 1.32 (m, 12H), 0.90 ppm (t, ^3J(H,H) = 6.6 Hz, 6H). ^{13}C NMR (400 MHz, $CDCl_3$, 25 °C, TMS): δ144.13, 140.25, 138.16, 131.69, 128.60, 127.98, 123.25, 120.00, 112.06, 99.49, 85.15, 36.01, 31.73, 31.25, 28.96, 22.63, 14.12 ppm. MS (MALDI-TOF): 558.0 [M^+]. HRMS (MALDI) *m*/*z* calcd for $C_{38}H_{38}S_2^{+1}$: 558.2409. Found: 558.2397. Elemental analysis calcd (%) for $C_{38}H_{38}S_2$: C 81.67, H 6.85. Found: C 81.65, H 7.03.

Synthesis of Compound 4a. Into a mixed solution of dry THF (75 mL) and tetramethylethylenediamine (TMEDA) (10 mL) cooled to −78 °C in a nitrogen atmosphere were added *n*-butyl lithium (2.4 M in hexane; 4.8 mL, 0.0115 mol), and the mixture was stirred at that temperature for 10 min. Then **3a** (1.505 g, 0.0038 mol) in dry THF (50 mL) was added dropwise. After stirring for 30 min at −78 °C, the mixture was added a solution of iodine (2.926 g, 0.0115 mol) in dry THF (50 mL) and stirred for another 15 min. After that, the solution was allowed to warm to room temperature for 20 h. Aqueous saturated sodium sulfite (Na_2SO_3) (100 mL) was added, and the resulting solid was collected by filtration and washed with water and methanol. Recrystallization from chlorobenzene afforded **4a** as yellow needle crystals (1.603 g, 65.0%). ^1H NMR (300 MHz, [D_4]DCB, 25 °C, TMS): δ 7.94 (s, 2H), 7.73 (m, 4H), 7.42 ppm (t, 6H). MS (MALDI-TOF): 642.0 [M^+]. HRMS (MALDI) *m*/*z* calcd for $C_{26}H_{12}I_2S_2^{+1}$: 641.8464, found 641.8484. Elemental analysis calcd (%) for for $C_{26}H_{12}I_2S_2$: C 48.62, H 1.88. Found: C 48.70, H 2.10.

Synthesis of Compound 4b. Compound **3b** (0.600 g, 0.0011 mol) was dissolved in dry THF (100 mL) and cooled to −78 °C under nitrogen. 2.4 M *n*-Butyl lithium in hexane (1.0 mL, 0.0024 mol) was added dropwise and the solution was stirred for 2 h at −78 °C. After that iodine (0.954 g, 0.0038 mol) was added and the solution mixture was kept stirring for 30 min at that temperature. Then, the solution was allowed to warm to room temperature for about 20 h and diluted with ether. The organic layer was washed with water, dried with magnesium sulfate, filtered, and concentrated to reddish solution (10 mL) which was added to an excess of methanol. The solid was collected and recrystallization from ethyl acetate gave **4b** as yellow needles (0.740 g, 85.0%). ^1H NMR (300 MHz, $CDCl_3$, 25 °C, TMS): δ 7.84 (s, 2H), 7.56 (d, ^3J(H,H) = 7.8 Hz, 4H), 7.23 (d, ^3J(H,H) = 7.8 Hz, 4H), 2.66 (t, ^3J(H,H) = 7.8 Hz, 4H), 1.65 (m, 4H), 1.33 (m, 12H), 0.90 ppm (t, ^3J(H,H) = 6.9 Hz, 6H). ^{13}C NMR (400 MHz, $CDCl_3$, 25 °C, TMS): δ 144.33, 144.26, 138.27, 132.91, 131.74, 128.59, 119.58, 109.04, 100.20, 84.32, 80.70, 36.01, 31.71, 31.21, 28.96, 22.62, 14.11 ppm. MS (MALDI-TOF): 809.9 [M^+]. HRMS (MALDI) *m*/*z* calcd for $C_{38}H_{36}S_2I_2^{+1}$: 810.0342, found 810.0319. Elemental analysis calcd (%) for $C_{38}H_{36}S_2I_2$: C 56.30, H 4.48. Found: C 56.24, H 4.41.

Synthesis of Compound 1a. To a solution of **4a** (0.800 g, 1.246 mmol), CuI (0.047 g, 0.246 mmol) and $PdCl_2(PPh_3)_2$ (0.175 g, 0.249 mmol) in THF (40 mL) were added phenylacetylene (0.305 g, 2.990 mmol) and triethylamine (10 mL) successively under nitrogen. The mixture was heated at 50 °C for about 12 h. After completing the reaction, the solution was removed. The residue was dissolved in chloroform (10 mL) and precipitated from excess methanol to get **1a**. Further purification through recrystallization from chlorobenzene gave yellow needles (0.474 g, 64.4%). Mp > 350 °C. ^1H NMR (300 MHz, [D_8]THF, 25 °C, TMS): δ 7.95 (s, 2H), 7.75 (m, 4H), 7.60 (m, 4H),

7.44 ppm (m, 12H). MS (MALDI-TOF): 590.1 [M^+]. HRMS (MALDI) m/z calcd for $C_{42}H_{22}S_2^{+1}$: 590.1157, found 590.1163. Elemental analysis calcd (%) for $C_{42}H_{22}S_2$: C 85.39, H 3.75. Found: C 85.31, H 3.98.

Synthesis of Compound 1b. Compound **1b** was synthesized in 60.2% yield in a manner similar to that of **1a** and purified by recrystallization from toluene. Mp 216 °C. ^{1}H NMR (300 MHz, $CDCl_3$, 25 °C, TMS): δ 7.83 (s, 2H), 7.70 (m, 4H), 7.49 (d, ^3J(H,H) = 7.8 Hz, 4H), 7.43 (m, 6H), 7.21 (d, ^3J(H,H) = 7.8 Hz, 4H), 2.64 (t, ^3J(H,H) = 7.5 Hz, 4H), 1.63 (m, 4H), 1.32 (m, 12H), 0.80 ppm (t, ^3J(H,H) = 6.9 Hz, 6H). ^{13}C NMR (400 MHz, $CDCl_3$, 25 °C, TMS): δ 144.29, 140.88, 138.16, 131.82, 131.58, 128.92, 128.57, 128.48, 127.45, 125.39, 122.64, 119.47, 111.13, 99.99, 96.93, 85.17, 82.59, 35.99, 31.69, 31.16, 28.94, 22.59, 14.09 ppm. MS (MALDI-TOF): 758.5 [M^+]. HRMS (MALDI) m/z calcd for $C_{54}H_{46}S_2^{+1}$: 758.3035, found 758.3045. Elemental analysis calcd (%) for $C_{54}H_{46}S_2$: C 85.44, H 6.11. Found: C 85.43, H 6.32.

Synthesis of Compound 1c. Compound **1c** was prepared in 63.7% yield in a manner similar to that described for **1a**: recrystallization from toluene. Mp 208 °C. ^{1}H NMR (300 MHz, $CDCl_3$, 25 °C, TMS): δ 7.85 (s, 2H), 7.59 (m, 8H), 7.39 (t, 6H), 7.24 (d, ^3J(H,H) = 8.4 Hz, 4H), 2.66 (t, ^3J(H,H) = 7.5 Hz, 4H), 1.65 (m, 4H; CH_2), 1.33 (m, 12H; CH_2), 0.9 ppm (t, ^3J(H,H) = 6.9 Hz, 6H). ^{13}C NMR (400 MHz, $CDCl_3$, 25 °C, TMS): δ 144.34, 140.85, 138.10, 131.74, 131.66, 128.92, 128.63, 128.45, 127.89, 125.01, 122.43, 119,72, 111.38, 100.43, 96.42, 84.58, 83.24, 36.02, 31.70, 31,22, 28.94, 22.61, 14.10 ppm. MS (MALDI-TOF): 758.6 [M^+]. HRMS (MALDI) m/z calcd for $C_{54}H_{46}S_2^{+1}$: 758.3035, found 758.3037. Elemental analysis calcd (%) for $C_{54}H_{46}S_2$: C 85.44, H 6.11. Found: C 85.41; H 6.07.

Synthesis of Compound 1d. Compound **1d** was synthesized in a manner similar to that described for **1a** and purified by flash chromatography on silica gel (petroleum ether eluent). Yield 66.1%. Mp 116 °C. ^{1}H NMR (300 MHz, $CDCl_3$, 25 °C, TMS): δ 7.82 (s, 2H), 7.60 (d, ^3J(H,H) = 7.5 Hz, 4H), 7.49 (d, ^3J(H,H) = 7.5 Hz, 4H), 7.24 (d, ^3J(H,H) = 7.5 Hz, 4H), 7.20 (d, ^3J(H,H) = 7.5 Hz, 4H), 2.65 (m, 8H), 1.64 (m, 8H), 1.32 (m, 24H), 0.89 ppm (m, 12H). ^{13}C NMR (400 MHz, $CDCl_3$, 25 °C, TMS): δ 144.16, 140.75, 138.05, 131.75, 131.59, 128.56, 128.53, 127.56, 125.17, 119.85, 119.60, 111.19, 100.30, 96.74, 84.72, 82.76, 36,01, 31.72, 31.23, 31.18, 28.99, 22.63, 14.12 ppm. MS (MALDI-TOF): 926.5 [M^+]. HRMS (MALDI) m/z calcd for $C_{66}H_{70}S_2^{+1}$: 926.4913, found 926.4916. Elemental analysis calcd (%) for $C_{66}H_{70}S_2$: C 85.48, H 7.61. Found: C 85.49, H 7.68.

Device Fabrication. OFET devices based on all target compounds **1a–d** were fabricated under ambient conditions without thermal annealing and adopted bottom-gate, top contact configuration. The substrate was a heavily doped, *n*-type Si gate electrode with a 300 nm thick SiO_2 layer (the specific capacitance was measured to be 10 nF cm^2) as the gate dielectric. **1a** was manufactured into single micrometer sized ribbon transistors on SiO_2/Si substrate, and the crystal was grew from chlorobenzene (50 °C), and **1b** and **1c** were fabricated into as-spun thin film devices using a > 1.0 wt % chloroform solution (3000 rpm, 30 s) respectively on OTS (octadecyltrichlorosilane) treated substrates. It was found that compound **1d** could not form successive thin films on OTS/SiO_2/Si substrate but could form crystalline films on SiO_2/Si substrate (optical micrograph, see the Supporting Information), so **1d** manufactured into devices with no OTS modified substrate. Additionally due to the low melting point (116 °C), the source and drain electrodes of **1d** transistors were processed by "gluing Au films" method.[19] As for devices **1b–1c**, all the channel lengths (L) were 31 μm with widths (W) of 273 μm, while for **1a** and **1d**, the W/L ratio ranged between 0.1 and 0.5 and 1–10, respectively. The mobility of the devices was calculated on the saturated region according to the expression $I_{DS} = (W/2L)\mu C_i(V_G - V_{Th})^2$, where I_{DS} is the drain-source current, μ is the field-effect mobility, and C_i is the capacitance. V_G and V_{th} are the gate voltage and threshold voltage, respectively.

■ ASSOCIATED CONTENT

Supporting Information

The CIF files of **1a–d** single crystals, the fluorescence spectra, the stimulated powder diffraction pattern of **1a–d** single crystals, the optical images of **1a** micrometer ribbons and **1d** thin films, the output and transfer curves of **1a–d** transistors, ^{1}H NMR and ^{13}C NMR spectra. This material is available free of charge via the Internet at http://pubs.acs.org.

■ AUTHOR INFORMATION

Corresponding Author

*E-mail: lhx@mail.sioc.ac.cn.

Author Contributions

§These authors contributed equally.

Notes

The authors declare no competing financial interest.

■ ACKNOWLEDGMENTS

This work was supported by National Natural Sciences Foundation of China (21190031) and National Basic Research Program of China (2011CB808405).

■ REFERENCES

(1) (a) Rotzoll, R.; Mohapatra, S.; Olariu, V.; Wenz, R.; Grigas, M.; Dimmler, K.; Shchekin, O.; Dodabalapur, A. *Appl. Phys. Lett.* **2006**, *88*, 123502. (b) Baude, P. F.; Ender, D. A.; Haase, M. A.; Kelley, T. W.; Muyres, D. V.; Theiss, S. D. *Appl. Phys. Lett.* **2003**, *82*, 3964.

(2) (a) Gelinck, G. H.; Huitema, H. E. A.; Van Veenendaal, E.; Cantatore, E.; chrijnemakers, S. L.; Van der Putten, J.; Geuns, T. C. T.; Beenhakkers, M.; Giesbers, J. B.; Huisman, B. H.; Meijer, E. J.; Benito, E. M.; Touwslager, F. J.; Marsman, A. W.; Van Rens, B. J. E.; De Leeuw, D. M. *Nat. Mater.* **2004**, *3*, 106. (b) Huitema, H. E. A.; Gelinck, G. H.; van der Putten, J. B. P. H.; Kuijk, K. E.; Hart, C. M.; Cantatore, E.; Herwig, P. T.; van Breemen, J. J. M.; de Leeuw, D. M. *Nature* **2001**, *414*, 599.

(3) (a) Rogers, J. A.; Bao, Z.; Baldwin, K.; Dodabalapur, A.; Crone, B.; Raju, V. R.; Kuck, V.; Katz, H.; Amundson, K.; Ewing, J.; Drzaic, P. *Proc. Natl. Acad. Sci. U. S. A.* **2001**, *98*, 4835. (b) Comiskey, B.; Albert, J. D.; Yoshizawa, H.; Jacobson, J. *Nature* **1998**, *394*, 253.

(4) (a) Sokolov, A. N.; Roberts, M. E.; Bao, Z. *Mater. Today* **2009**, *12*, 12. (b) Sokolov, A. N.; Tee, B. C. K.; Bettinger, C. J.; Tok, J. B. H.; Bao, Z. *Acc. Chem. Res.* **2012**, *45*, 361.

(5) Some reviews see: (a) Anthony, J. E. *Chem. Rev.* **2006**, *106*, 5028. (b) Murphy, A. R.; Frechet, J. M. J. *Chem. Rev.* **2007**, *107*, 1066. (c) Zaumseil, J.; Sirringhaus, H. *Chem. Rev.* **2007**, *107*, 1296. (d) Wen, Y.; Liu, Y. *Adv. Mater.* **2010**, *22*, 1331. (e) Meng, Q.; Dong, H.; Hu, W.; Zhu, D. *J. Mater. Chem.* **2011**, *21*, 11708. (f) Usta, H.; Facchetti, A.; Marks, T. J. *Acc. Chem. Res.* **2011**, *44*, 501. (g) Wang, C.; Dong, H.; Hu, W.; Liu, Y.; Zhu, D. *Chem. Rev.* **2012**, *112*, 2208.

(6) Bredas, J. L.; Calbert, J. P.; da Silva, D. A.; Cornil, J. *Proc. Natl. Acad. Sci. U.S.A.* **2002**, *99*, 5804.

(7) Moon, H.; Zeis, R.; Borkent, E. J.; Besnard, C.; Lovinger, A. J.; Siegrist, T.; Kloc, C.; Bao, Z. *J. Am. Chem. Soc.* **2004**, *126*, 15322.

(8) Mattheus, C. C.; de Wijs, G. A.; de Groot, R. A.; Palstra, T. T. M. *J. Am. Chem. Soc.* **2003**, *125*, 6323.

(9) Wang, C.; Dong, H.; Li, H.; Zhao, H.; Meng, Q.; Hu, W. *Cryst. Growth Des.* **2010**, *10*, 4155.

(10) (a) Miao, Q.; Chi, X.; Xiao, S.; Zeis, R.; Lefenfeld, M.; Siegrist, T.; Steigerwald, M. L.; Nuckolls, C. *J. Am. Chem. Soc.* **2006**, *128*, 1340. (b) Li, Y.; Wu, Y.; Liu, P.; Prostran, Z.; Gardner, S.; Ong, B. S. *Chem. Mater.* **2007**, *19*, 418. (c) Ponomarenko, S. A.; Tatarinova, E. A.; Muzafarov, A. M.; Kirchmeyer, S.; Brassat, L.; Mourran, A.; Moeller, M.; Setayesh, S.; de Leeuw, D. *Chem. Mater.* **2006**, *18*, 4101. (d) Roncali, J.; Leriche, P.; Cravino, A. *Adv. Mater.* **2007**, *19*, 2045.

(11) Zen, A.; Bilge, A.; Galbrecht, F.; Alle, R.; Meerholz, K.; Grenzer, J.; Neher, D.; Scherf, U.; Farrell, T. *J. Am. Chem. Soc.* **2006**, *128*, 3914.

(12) Wang, C.; Liu, Y.; Ji, Z.; Wang, E.; Li, R.; Jiang, H.; Tang, Q.; Li, H.; Hu, W. *Chem. Mater.* **2009**, *21*, 2840.
(13) Hur, J. A.; Bae, S. Y.; Kim, K. H.; Lee, T. W.; Cho, M. J.; Choi, D. H. *Org. Lett.* **2011**, *13*, 1948.
(14) (a) Hundt, N.; Palaniappan, K.; Servello, J.; Dei, D. K.; Stefan, M. C.; Biewer, M. C. *Org. Lett.* **2009**, *11*, 4422. (b) Sista, P.; Nguyen, H.; Murphy, J. W.; Hao, J.; Dei, D. K.; Palaniappan, K.; Servello, J.; Kularatne, R. S.; Gnade, B. E.; Xue, B.; Dastoor, P. C.; Biewer, M. C.; Stefan, M. C. *Macromolecules* **2010**, *43*, 8063.
(15) Zhang, X.; Johnson, J. P.; Kampf, J. W.; Matzger, A. J. *Chem. Mater.* **2006**, *18*, 3470.
(16) The long absorption tail into the NIR region was partailly caused by the light scattering.
(17) Gao, X.; Wu, W.; Liu, Y.; Jiao, S.; Qiu, W.; Yu, G.; Wang, L.; Zhu, D. *J. Mater. Chem.* **2007**, *17*, 736.
(18) Meng, Q.; Jiang, L.; Wei, Z.; Wang, C.; Zhao, H.; Li, H.; Xu, W.; Hu, W. *J. Mater. Chem.* **2010**, *20*, 10931.
(19) Jiang, L.; Dong, H.; Hu, W. *J. Mater. Chem.* **2010**, *20*, 4994.